How to Cite: Avazova, O.B., Pirniyazov, K.K., & Rashidova, S.Sh. (2026). Rheological Properties of the Polymeric Preparative Form of Chitosan Nanoascorbate from *Bombyx mori*. *Eurasian Journal of Chemistry.* https://doi.org/10.31489/2959-0663/2-26-11

Article

Received: 26 March 2026 | Revised: 22 May 2026 | Accepted: 2 June 2026 | Published online: 3 June 2026

UDC 547.9:541.64

https://doi.org/10.31489/2959-0663/2-26-11

Oynavod B. Avazova, Kudrat K. Pirniyazov*, Sayyora Sh. Rashidova

Institute of Polymer Chemistry and Physics, Academy of Sciences of the Republic of Uzbekistan, Tashkent, Uzbekistan
*(*Corresponding author's e-mail: qudratpirniyazov8875@gmail.com)*

Rheological Properties of the Polymeric Preparative Form of Chitosan Nanoascorbate from *Bombyx mori*

Chitosan nanoascorbate samples were synthesized by controlling the pH of the solution and the ratio of the initial components: ascorbic acid and chitosan derived from *Bombyx mori*. In this study, the rheological properties of polymeric preparative forms based on chitosan nanoascorbate and methylhydroxyethylcellulose systems at different concentrations were investigated. The chitosan nanoascorbate samples were obtained by regulating the ratio of Bombyx mori chitosan to ascorbic acid and adjusting the pH of the reaction medium during the synthesis process. In the initial 0.025 % chitosan nanoascorbate solution, the viscosity increased from 0.33 Pa·s to 4.14 Pa·s under shear, indicating possible hydrodynamic clustering and the formation of temporary aggregates between nanoparticles. In dilute systems containing 0.0125 % chitosan nanoascorbate and 0.1 % methylhydroxyethylcellulose, the viscosity increased from 3.1 Pa·s to 5.0 Pa·s, suggesting interactions between polymer chains and nanoparticles, although a fully developed spatial network was not formed. In the system with intermediate concentrations (0.025 % chitosan nanoascorbate : 0.2 % methylhydroxyethylcellulose), the viscosity varied from 6.2 Pa·s to 10.9 Pa·s and exhibited near-Newtonian flow behavior. In the system with the highest concentration (0.05 % chitosan nanoascorbate : 0.4 % methylhydroxyethylcellulose), the viscosity decreased from 45 Pa·s to 18 Pa·s, indicating pseudoplastic behavior and the partial disruption of the three-dimensional spatial network under shear. Frequency analysis and the Power-law model confirmed the viscosity and elastic properties of these two types of systems.

Keywords: chitosan nanoascorbate, *Bombyx mori*, polymeric preparative form, storage modulus, loss modulus, consistency coefficient, flow behavior index, dynamic viscosity, shear stress

1 Introduction

Polycationic and polyanionic polysaccharides found in marine algae, crustaceans, and insects are considered promising sources of biologically active compounds. Among these natural biopolymers, chitosan (CS) is of particular interest. CS is a non-toxic, biocompatible, and biodegradable polysaccharide that exhibits antimicrobial, antioxidant, and immunostimulating properties. In addition, CS can be used in medicine as a material that promotes rapid wound healing and participates in tissue regeneration processes, as well as a carrier for biologically active compounds such as ascorbic acid (AA) [1–3]. In agriculture, CS and its derivatives are used as agents for combating plant and animal diseases and as growth stimulants [4]. It is well known that CS is insoluble in water due to strong intermolecular interactions and hydrogen bonding between macromolecules; however, it dissolves readily in dilute organic acids. Therefore, the preparation of water-soluble derivatives of CS significantly expands its applications in agriculture, biotechnology, and medicine [3, 5]. Among these derivatives, chitosan ascorbate (CSA), a salt formed with ascorbic acid (AA), and its nanostructured form, chitosan nanoascorbate (CSNA), exhibit high biological activity. These materials have been reported to possess wound-healing, antimicrobial, and plant growth-stimulating properties [4, 6].

The synthesized CSA and CSNA samples are environmentally safe and exhibit antimicrobial activity against diseases occurring in plant and animal organisms [6, 7]. The investigation of the interaction mechanisms between CS and AA is currently one of the important scientific issues, since the interaction processes between CS and AA strongly depend on the pH of the medium and temperature. According to the literature data [8, 9], the formation of CSA compounds can proceed via three main mechanisms. In the first mechanism, covalent donor–acceptor complexes are formed. This interaction is based on the interaction between the enolic hydroxyl (OH) group located at the C3 carbon of AA and the amino (NH_2) groups of CS. The reaction proceeds in an aqueous medium at room temperature. In this case, the lactone ring of AA remains intact, while the amino groups of CS are in a protonated state [8].

In the literature, it has been reported that at pH 5–6.5 and a temperature of approximately 25 °C, the interaction between chitosan and ascorbic acid in aqueous solution over more than 6 hours may lead to the formation of a covalent imine (Schiff base) linkage [9, 10]. This can be explained by the fact that ascorbic acid, in the presence of dissolved oxygen in aqueous media, is partially oxidized to dehydroascorbic acid, which contains reactive carbonyl groups. It should be noted that ascorbic acid is unstable in aqueous solution, and its enolic form is readily susceptible to oxidation depending on the reaction conditions. Therefore, the interaction between amino groups of chitosan and carbonyl groups (including those formed via oxidation of ascorbic acid to dehydroascorbic acid) results in the formation of an imine (Schiff base) linkage between chitosan and ascorbic acid [10].

The third mechanism proceeds through the thermal opening of the lactone ring of AA. Under an inert nitrogen atmosphere at 60–70 °C and pH 6–7, the opening of the lactone ring of AA leads to the formation of carboxyl (COO^-) groups. These groups react with the amino groups of CS, resulting in the formation of covalent amide bonds. The formation of these bonds has been confirmed in the literature by NMR spectroscopy [11, 12].

In addition, chitosan nanoascorbate (CSNA) is commonly obtained by forming nanostructured complexes of CS with AA using the ionotropic gelation method in the presence of sodium tripolyphosphate (STPP). In this process, nanoparticles are formed due to electrostatic interactions between the protonated positively charged amino groups of CS and the negatively charged phosphate groups of STPP. The size of the nanoparticles mainly depends on the acid concentration and the degree of deacetylation (DD) of CS. CS with a higher DD contains a greater number of free amino groups, which increases the charge density and consequently the number of effective electrostatic cross-linking sites with STPP [13].

Although the biological properties of chitosan nanoderivatives have been widely studied, information in the literature on obtaining polymeric preparative forms of chitosan nanoderivatives based on AA and their application in sericulture remains limited [14]. Therefore, in the present study, a polymeric preparative form of CSNA was obtained in the presence of a methylhydroxyethylcellulose (MHEC) solution for potential application in sericulture. MHEC was selected because of its low toxicity, easy biodegradability in nature, and its ability to preserve the activity of CSNA**.** In addition, MHEC acts as an effective thickening agent for the formation of polymeric preparative formulations.

Currently, various polymer-based preparations are used to control diseases of the silkworm and to stimulate its growth and development. These preparations are mainly produced in powder, gel, and solution forms. In addition to their biochemical activity, it is also important to evaluate the resistance of these formulations to physical and mechanical effects during their application.

In addition, the spraying technology of preparations plays an important role in the effective application of pesticides, biopreparations, and plant protection agents in agriculture. During the spraying process, the physicochemical and rheological properties of the solution determine droplet formation, droplet size, adhesion to leaf surfaces, and dispersion behavior in the atmosphere. Therefore, in recent years, the investigation of the rheological properties of formulation systems has become an important research direction in agrochemistry and chemical sciences.

According to the literature, the rheological properties of spraying solutions significantly influence the atomization and dispersion mechanisms of droplets. In particular, an increase in solution viscosity leads to an increase in droplet diameter, which in turn reduces the efficiency of spraying [15].

At the same time, the addition of polymeric agents can modify the viscoelastic properties of the solutions, thereby improving the stability of droplets during the spraying process [16]. In spraying technology, the viscosity and surface tension of the solution are considered the main parameters. Studies have shown that solutions with low viscosity undergo atomization more easily and form smaller droplets. However, such droplets can disperse more readily in the atmosphere, which may reduce the efficiency of the applied preparation. Conversely, solutions with higher viscosity form larger droplets that exhibit better retention on plant surfaces [17].

In recent years, the use of polymer-based adjuvants has been considered one of the effective approaches for improving spraying technology. The long-chain structure of polymer molecules limits droplet breakup and enhances spray stability. This behavior is closely related to the non-Newtonian rheological properties of polymer solutions, in which the flow mechanism depends on the applied shear rate [18]. The pseudoplastic behavior of polymer solutions is associated with the alignment and deformation of macromolecular chains under shear flow, accompanied by a reduction in intermolecular interactions. As a result, an increase in shear rate leads to a decrease in apparent viscosity. This effect plays an important role in spraying systems, where reduced viscosity during pumping facilitates atomization [19]. In contrast, certain polymer and colloidal sys-

tems may exhibit dilatant behavior, where increasing shear rate intensifies particle interactions and leads to the formation of transient structures, resulting in increased viscosity.

In agrochemical formulations, solutions with optimized rheological properties ensure uniform spreading and retention on plant surfaces. Therefore, recent studies focus on key rheological parameters such as the consistency coefficient and flow behavior index. It has been demonstrated that controlling solution viscosity using polymer adjuvants improves droplet size distribution and enhances biological efficiency [19–21]. In addition, chitosan-based systems are widely studied due to their unique physicochemical properties, biocompatibility, and ability to form stable nano-sized structures [22–24]. Particularly, chitosan nanoparticles and their derivatives, including antioxidant-modified systems such as nanoascorbates, demonstrate enhanced stability and functional performance in solution [24, 25]. Furthermore, biomacromolecules derived from Bombyx mori, such as silk fibroin, are extensively used in the design of advanced polymeric systems due to their structural stability, biodegradability, and excellent mechanical properties [26, 27].

Thus, the rheological properties of spray solutions, including viscosity and non-Newtonian flow behavior, represent critical factors governing droplet formation and deposition efficiency on plant surfaces. Control of these parameters is essential for optimizing spraying performance and improving the effectiveness of agrochemical formulations. The main aim of this study was to obtain a polymeric preparative form of chitosan nanoascorbate (CSNA) derived from Bombyx mori and to investigate its rheological properties. Particular attention was given to evaluating the influence of component concentration on the flow behavior and structural characteristics of the system. Chitosan nanoascorbate (CSNA) represents a promising functional biopolymer system that combines antioxidant activity with tunable rheological properties, making it a potential candidate for the development of advanced spraying formulations with enhanced stability and performance.

2 Experimental

2.1 Synthesis of Chitosan Nanoascorbate Samples

In this study, CS derived from *Bombyx mori* (*B.M.*) silkworm pupae with a molecular weight of 140 kDa and a degree of deacetylation (DD) of 84 % was used. The molecular weight of chitosan was determined by viscometry using the Mark–Houwink equation based on intrinsic viscosity [1]. The intrinsic viscosity was obtained by extrapolation from the plot of reduced viscosity versus solution concentration. In addition, the molecular weight of chitosan nanoascorbate was determined using the dynamic light scattering (DLS) method. The DD of the initial CS samples was determined by conductometric titration in 0.1 N hydrochloric acid using a *Mettler Toledo* conductometer (USA). CS was obtained from *B.M.* silkworm pupae through deproteinization, demineralization, and subsequent deacetylation in a 50 % sodium hydroxide solution at 120 °C for 3 h. This process was carried out in the pilot-scale facility of the Institute of Polymer Chemistry and Physics of the Academy of Sciences of the Republic of Uzbekistan following the procedure described in the literature [1].

CSNA was synthesized in an aqueous medium by the ionotropic gelation method. During the process, a 0.5 % solution of STPP was used as a stabilizing agent based on electrostatic interactions. The synthesis was carried out by controlling the ratios of the initial components and the pH of the solution. To determine the amount of unreacted (free) ascorbic acid in the reaction system, the liquid phase was separated by centrifugation. The ascorbic acid (AA) content in CSNA was calculated based on the determination of free AA in the liquid phase by alkaline titration using phenolphthalein as an indicator. The degree of AA binding was calculated according to the ratio (M_{AA})exp./(M_{AA})calc. [24].

The obtained products were freeze-dried at −48 °C for 5–6 h using an "*Alpha Christ*" lyophilizer (Germany). The yield of the final products was evaluated as the ratio of the calculated mass to the experimentally obtained mass of the substance. The component ratios were calculated based on the molar concentrations of the initial substances. In all syntheses, a 0.05 M aqueous solution of ascorbic acid was used, while the concentration of chitosan was set at 0.2 M. The volume of the stabilizer (STPP) was determined based on its molar ratio relative to the other components. The pH of the reaction system was measured at the end of the synthesis at 25 °C using a *Bante-210* pH meter (China). Solutions of AA, the titrant, and STPP were prepared using an analytical procedure: the exact dry mass of the substances was weighed on an analytical balance, dissolved in distilled water, and stirred with a magnetic stirrer until complete dissolution.

2.2 Preparation of Solutions for Rheological Measurements

In the experiments, polymeric preparative forms based on CSNA and MHEC were prepared using their solutions in 2 % acetic acid at different concentrations. The studied systems included: No. 1 — 0.2 %

MHEC; No. 2 — 0.025 % CSNA; No. 3 — 0.0125 % CSNA and 0.1 % MHEC; No. 4 — 0.025 % CSNA and 0.2 % MHEC; and No. 5 — 0.05 % CSNA and 0.4 % MHEC. During the preparation of the solutions, accurately weighed amounts of the components were dissolved in 2 % acetic acid and stirred for 24 h using a magnetic stirrer until complete dissolution.

2.3 Rheological Measurement Method

The rheological properties of the samples were studied using an Anton Paar MCR 92 rotational rheometer (Austria). During shear flow of the solutions, macromolecular chains undergo deformation-induced orientation, and the samples exhibit non-Newtonian flow behavior over a wide concentration range. The rheological properties of CSNA samples were investigated using a cylindrical measuring system. The rheometer allows measurements to be performed in both rotational and oscillatory modes. To evaluate the structural characteristics and deformation behavior of the samples, the variation of shear stress (τ) was monitored during the increase and decrease of the shear rate (γ). Based on the obtained results, the rheological behavior of the solutions was analyzed.

Rheological measurements were performed using an Anton Paar MCR 92 rheometer under controlled temperature conditions (±0.1 °C). The instrument operates with a high level of precision, where the relative error in viscosity measurements does not exceed ±1 %, and the accuracy of shear stress determination is within ±0.5–1 %, according to the manufacturer's specifications.

These instrumental parameters ensure reliable and reproducible determination of viscoelastic properties. However, statistical error analysis (e.g., standard deviation) was not applied in this study, as replicate measurements for individual data points were not performed. Therefore, graphical data are presented as single experimental values with high instrumental accuracy rather than statistically averaged datasets.

2.4 Dynamic Light Scattering (DLS) Analysis

Particle size determination was carried out using dynamic light scattering (DLS) on a *BeNano 90* instrument (China). CSNA samples were dissolved in 2 % acetic acid at a concentration of 0.25 % and kept at room temperature (~25 °C) for approximately 24 h until complete dissolution was achieved. DLS measurements were not performed at a concentration of 0.025 % due to the inherent sensitivity limits of the DLS technique and the dependence of scattering intensity on particle size and concentration, which results in a low signal-to-noise ratio and unreliable measurements. Prior to measurement, the solutions were filtered through a microporous membrane filter (pore size 10–20 μm) to remove large particles and prevent clogging of the DLS cuvette. The filtered solution was transferred into a DLS cuvette (up to 1 ml), and measurements were performed to determine the average hydrodynamic diameter and particle size distribution. Each measurement was repeated 3–5 times to ensure statistical reliability. Based on the hydrodynamic diameter, the molecular weight (M) of the polymer was estimated using the following relationship:

$$Rh = k\,M^{\nu}, \tag{1}$$

where: M — is the molecular weight of the polymer (g/mol); k — is the empirical coefficient specific to the polymer and solvent; ν — is a scaling exponent dependent on the polymer chain conformation.

The values of k and ν were determined using standards of known molecular weight.

2.5 Atomic Force Microscopy (AFM) Analysis of CSNA

The morphology and particle size of CSNA were analyzed using atomic force microscopy (AFM) on an Agilent 5500 instrument (Agilent, USA). Silicon cantilevers with a spring constant of 9.5 $N \cdot m^{-1}$ and a resonant frequency of 145 kHz were used.

For sample preparation, diluted aqueous solutions of CSNA were deposited onto a clean glass substrate and allowed to dry under ambient conditions prior to analysis.

3 Results and Discussions

3.1 Results of DLS Analysis: Particle Size Distribution and Molecular Weight of CSNA, MHES, and Polymeric Preparative Forms

For this purpose, dynamic light scattering (DLS) measurements were performed using a BeNano 90 instrument. The molecular weight and particle size distribution of CSNA in solution were evaluated using samples synthesized at an initial component molar ratio of CS:AA:STPP = 4:1:0.25. The results showed that particles in the 0.025 % CSNA solution were distributed within the size range of 220–651 nm. The average hydrodynamic diameter was 567 nm, while the main peak in the DLS profile was observed at approximately 360 nm, indicating that particles with an average size of around 360 nm are predominant in the system.

Analysis of the particle size distribution revealed that approximately 50 % of the particles have a diameter of about 320 nm. It should be noted that in the present study, the term “nanoascorbate” is used not solely with respect to the geometric size of the particles, but rather to their nanostructured nature. The particle sizes in the range of 200–700 nm determined by DLS represent the hydrodynamic diameter of aggregates formed in solution. These aggregates consist of primary nanoscale domains formed as a result of ionotropic gelation and intermolecular interactions. Therefore, despite the overall particle size exceeding 100 nm, the system can be considered nanostructured in nature [28]. The obtained results are presented in (Fig. 1).

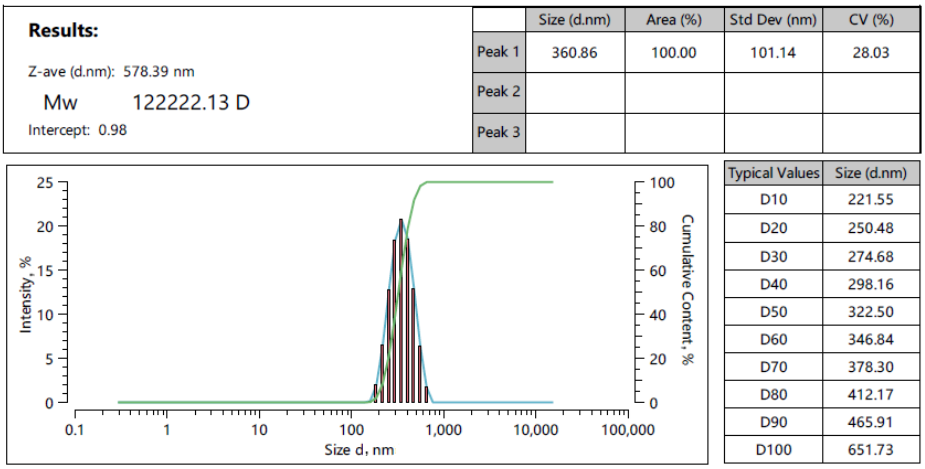

	Size (d.nm)	Area (%)	Std Dev (nm)	CV (%)
Peak 1	360.86	100.00	101.14	28.03
Peak 2				
Peak 3				

Typical Values	Size (d.nm)
D10	221.55
D20	250.48
D30	274.68
D40	298.16
D50	322.50
D60	346.84
D70	378.30
D80	412.17
D90	465.91
D100	651.73

Figure 1. Results of DLS analysis: particle size distribution and molecular weight of a 0.25 % CSNA solution

MHEC was used as an auxiliary component in the preparation of the polymer preparative form of CSNA in order to regulate the viscosity of the solution. MHEC is a cellulose derivative that, unlike chitosan, does not contain amino groups and is mainly composed of hydroxyl (–OH), methoxy (–OCH_3), and hydroxyethyl (–OCH_2CH_2OH) ether groups. Therefore, MHEC is a neutral, non-ionic polymer that is soluble in water and some organic solvents. As a result, the DLS behavior of MHEC solutions differs significantly from that of chitosan solutions. MHEC does not interact chemically with acetic acid due to the absence of amino groups. Furthermore, since MHEC does not contain carboxyl groups typical of acidic compounds, it does not chemically interact with the amino groups of CSNA. However, in diluted solutions, acetic acid partially dissociates into ions, which may weaken and rearrange intermolecular hydrogen bonds between macromolecules, potentially leading to phase separation and the formation of two distinct phases. According to the DLS results, the particle size distribution of the 0.25 % MHEC solution prepared in 2 % acetic acid showed that the particle sizes were mainly in the range of 740–2672 nm (Figure 2).

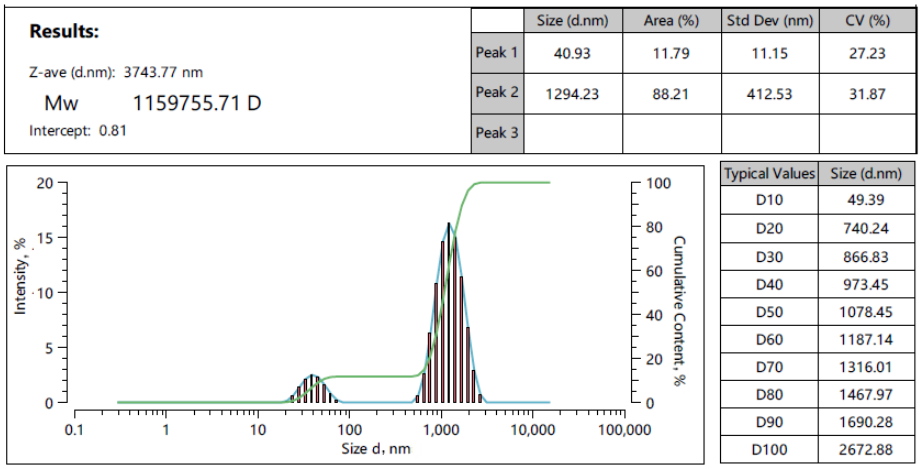

	Size (d.nm)	Area (%)	Std Dev (nm)	CV (%)
Peak 1	40.93	11.79	11.15	27.23
Peak 2	1294.23	88.21	412.53	31.87
Peak 3				

Typical Values	Size (d.nm)
D10	49.39
D20	740.24
D30	866.83
D40	973.45
D50	1078.45
D60	1187.14
D70	1316.01
D80	1467.97
D90	1690.28
D100	2672.88

Figure 2. DLS results and particle size distribution of the 0.2 % MHEC solution

It can be concluded that, in the polymeric preparative form (PPF) of the CSNA solution, particles in the size range of 300–400 nm correspond to CSNA macromolecules, since such particles were not observed in the MHEC solution. In contrast, particles in the range of 700–2672 nm can be attributed to MHEC macromolecular structures. Analysis of the particle size distribution showed that less than 20 % of the particles fall within the 295–442 nm range, which can be associated with the presence of nanoscale CSNA structures within the polymeric preparative form. The obtained results are presented in Figure 3.

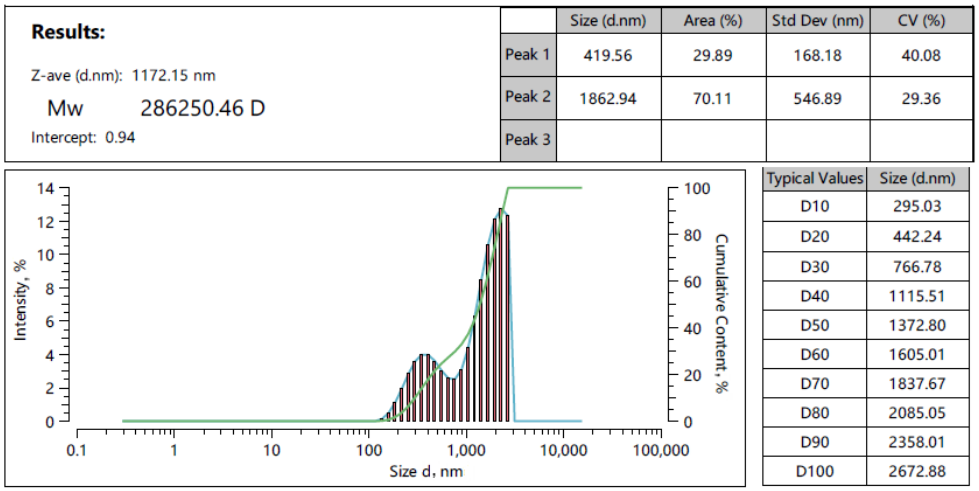

Figure 3. DLS results and particle size distribution of the CSNA PPF solution (CSNA 0.025 % and MHES 0.2 %)

3.2 Atomic Force Microscopy (AFM) Results

The obtained AFM results confirm the presence of particles with sizes ranging from 200 to 700 nm in the composition of chitosan nanoascorbate. The results are presented in Figure 4.

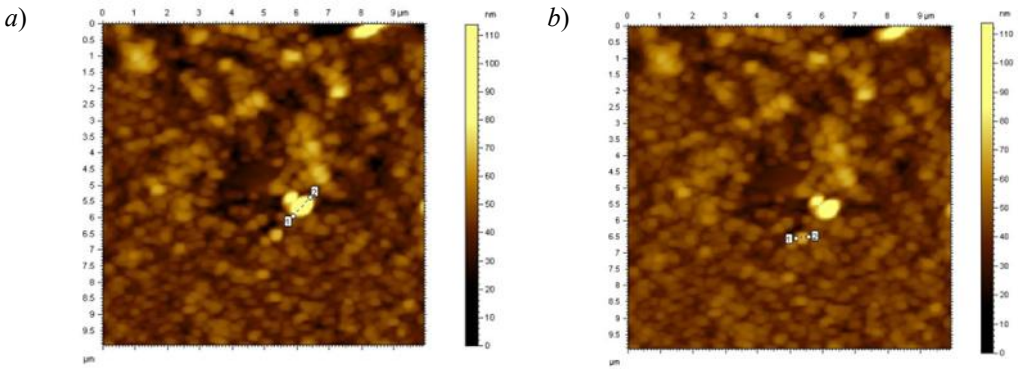

Figure 4. AFM images of CSNA obtained on a pilot-scale unit (CS:AA:STPP = 4:1:0.25): (*a*) particle size up to 709 nm; (*b*) particle size up to 200 nm

The AFM results are in good agreement with the particle sizes determined by DLS for the CSNA samples. In particular, according to the DLS analysis, the particle size of CSNA samples was found to be in the range of 220–651 nm, whereas AFM analysis showed a size range of 200–700 nm. Furthermore, due to the relatively large particle size and molecular weight of MHEC, the polymeric preparative form of CSNA and MHEC samples were not analyzed by AFM.

3.3 Rheological Properties of CSNA and Its Polymeric Preparative Formulation Solutions

The polymeric preparative formulation based on chitosan nanoascorbate (CSNA) is applied in solution form via spray application onto mulberry leaves and silkworms. During this process, viscosity (η) plays a crucial physicochemical role, as it directly influences droplet formation, dispersion behavior, surface adhesion, and ultimately the biological efficiency of the formulation. Therefore, the resistance of CSNA-based systems to mechanical deformation during spraying, as well as their viscosity characteristics, was investigated using rheological measurements.

In the rheological study, an amplitude sweep test was first performed to evaluate the response of the prepared solutions to increasing mechanical deformation. Based on the obtained results, the dependences of the storage modulus (G') and loss modulus (G'') on strain amplitude (γ, %) were plotted (Fig. 5).

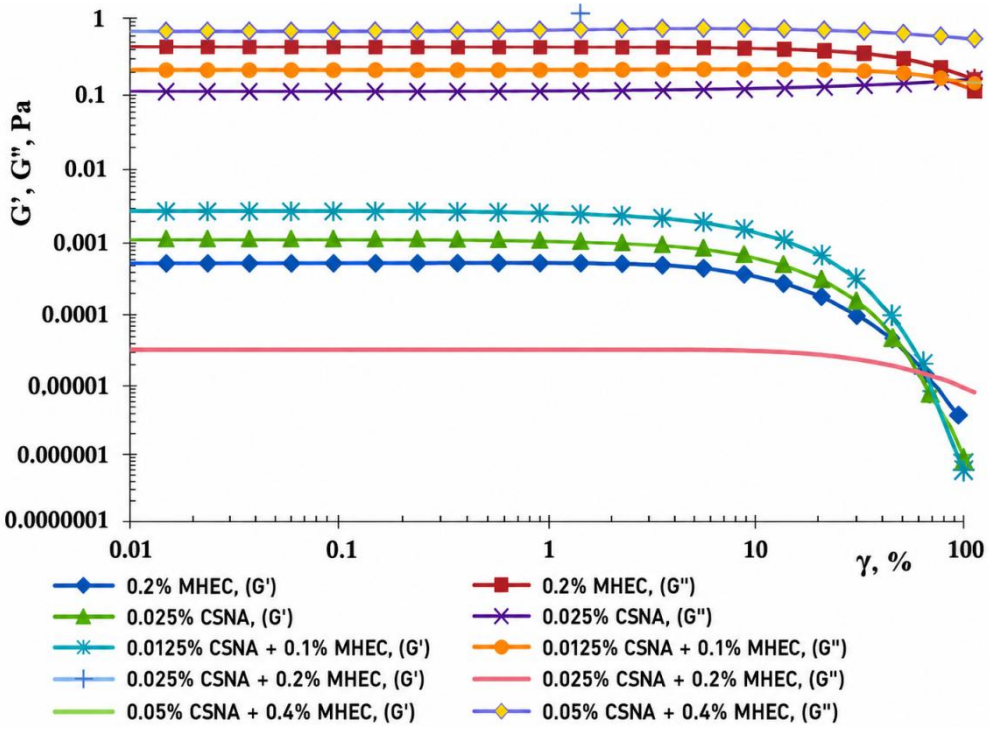

Figure 5. Dependence of storage (G') and loss (G'') moduli on shear strain amplitude (γ, %):
(*1*) 0.2 % MHEC; (*2*) 0.025 % CSNA; (*3*) 0.0125 % CSNA + 0.1 % MHEC; (*4*) 0.025 % CSNA + 0.2 % MHEC;
(*5*) 0.05 % CSNA + 0.4 % MHEC

As shown in Fig. 5, all studied systems exhibit G″ values higher than G′ within the shear strain range up to approximately 10 %, indicating the predominance of viscous behavior in this region. This indicates that the samples exhibit a sol/viscoelastic liquid structure, in which the internal structure remains weakly developed in the initial state. The systems behave as viscoelastic fluids, demonstrating both elastic and viscous responses. This behavior suggests the presence of transient macromolecular network formation and significant intermolecular interactions.

With increasing strain amplitude (γ) in the range of 20–100 %, the value of G′ decreases sharply, while G″ decreases more gradually. Under these conditions, structural disruption occurs in the samples, leading to a transition from a more elastic state to a predominantly liquid-like behavior.

Sample No. 1 exhibits pronounced elastic behavior, where G′ decreases from approximately 7.6×10^{-4} to 7.13×10^{-7}, while G'' decreases from about 0.589 to 0.122. This indicates the presence of a highly interconnected elastic structure in the system. Samples No. 2 and No. 3 show semi-elastic behavior, with the initial values of G' and G'' being lower than those of sample No. 1. These systems are characterized by a moderately branched structure and relatively high chain mobility. Samples No. 4 and No. 5 behave as highly viscous systems with increased internal friction. In sample No. 5, the value of G'' is relatively high (around 0.613), indicating significant dissipative energy loss within the system. This suggests rapid molecular rearrangement processes. For all samples, the structural disruption region under deformation occurs within the strain amplitude range of approximately $\gamma \approx 6$–10 %. No intersection between G' and G'' was observed for any of the samples, indicating that the systems did not undergo a transition to a purely liquid state and retained their gel-like behavior.

As shown in Table 1, for samples No. 1–5, the dominance of G'' over G' ($G'' > G'$) was observed across the entire frequency range. In particular, for samples 1–3 at low frequencies ($\omega \approx 0.3$–1 rad/s), the values of G' were in the range of 10^{-7}–10^{-6} Pa, whereas G'' reached 10^{-2}–10^{-1} Pa. As a result, the loss tangent ($\tan\delta = G''/G'$) reached values up to approximately 20000. Although both G'' and G' increased proportionally, the G' values remained extremely low (10^{-7}–10^{-5} Pa).

Table 1

Frequency dependence of storage modulus (*G′*) and loss modulus (*G″*) for samples No. 1–5

ω	No. 1		No. 2		No. 3		No. 4		No. 5	
(rad/s)	*G'*	*G"*	*G'*	*G"*	*G'*	*G"*	*G'*	*G"*	*G'*	*G"*
0.314	3.22E-07	0.006	4.86E-07	0.010	1.19E-07	0.002	0.000	0.004	0.010	0.022
0.521	5.58E-07	0.011	3.20E-07	0.006	5.45E-07	0.011	6.38E-07	0.013	0.005	0.032
0.866	1.93E-04	0.025	4.86E-07	0.010	4.57E-07	0.009	1.07E-06	0.021	0.004	0.048
1.440	1.32E-06	0.026	1.13E-06	0.023	1.24E-06	0.025	1.27E-06	0.025	0.005	0.078
2.380	2.52E-06	0.050	1.61E-06	0.032	1.13E-06	0.023	2.32E-06	0.046	0.013	0.131
3.960	4.01E-06	0.080	2.78E-06	0.056	5.90E-07	0.012	3.60E-06	0.072	0.015	0.214
6.570	6.93E-06	0.139	8.17E-06	0.163	4.53E-06	0.091	6.44E-06	0.129	0.002	0.342
10.900	1.27E-05	0.255	4.62E-06	0.092	8.52E-06	0.170	1.42E-05	0.284	2.85E-05	0.570
18.100	2.60E-05	0.519	1.13E-05	0.226	1.65E-05	0.330	2.94E-05	0.587	4.77E-05	0.954
30.000	5.84E-05	1.168	3.90E-05	0.780	3.27E-05	0.653	7.13E-05	1.427	8.64E-05	1.728
49.900	1.38E-04	2.761	9.63E-05	1.926	6.58E-05	1.316	1.80E-04	3.603	1.65E-04	3.299
82.800	3.38E-04	6.764	2.26E-04	4.525	1.30E-04	2.603	4.52E-04	9.049	3.76E-04	7.525
137.000	8.69E-04	17.380	6.33E-04	12.663	3.86E-04	7.715	1.19E-03	23.776	8.66E-04	17.321
228.000	3.15E-03	62.986	3.05E-03	61.080	2.12E-03	42.473	4.12E-03	82.355	3.20E-03	63.927
379.000	8.39E-03	167.870	5.06E-03	101.110	6.46E-03	129.200	9.86E-03	197.090	9.37E-03	187.370
628.000	6.87E-02	1374.100	6.00E-02	1200.100	6.54E-02	1309.000	6.01E-02	1202.700	5.86E-02	1171.500

Based on the data presented in Table 1, the corresponding graph is shown in Figure 6. Analysis of the graph indicates that samples 1–3 exhibit predominantly viscous behavior, with no formation of a three-dimensional network structure, and free relaxation of macromolecular chains is observed. With increasing frequency, the *G″* values increase exponentially, indicating restricted molecular mobility under dynamic conditions. However, the very low values of *G′* confirm the instability of the network formation mechanism and indicate that the systems exist as viscous liquid dispersions. In these samples, the dominance of *G″* results in pronounced flow behavior and relatively short relaxation times.

These solutions can be easily sprayed onto mulberry leaves without clogging the nozzle. However, a limitation of samples No. 1–3 is the very high tan δ values, indicating a predominantly liquid phase. As a result, after deposition on the leaf surface the solution may exhibit low adhesion and may partially flow off, leading to non-uniform coverage.

In contrast, for samples No. 4 and No. 5, at low frequencies (0.314–3.96 rad s^{-1}) the values of *G′* ≈ 0.009–0.015 Pa and *G″* ≈ 0.02–0.21 Pa is relatively close, with tan δ ≈ 2–15.

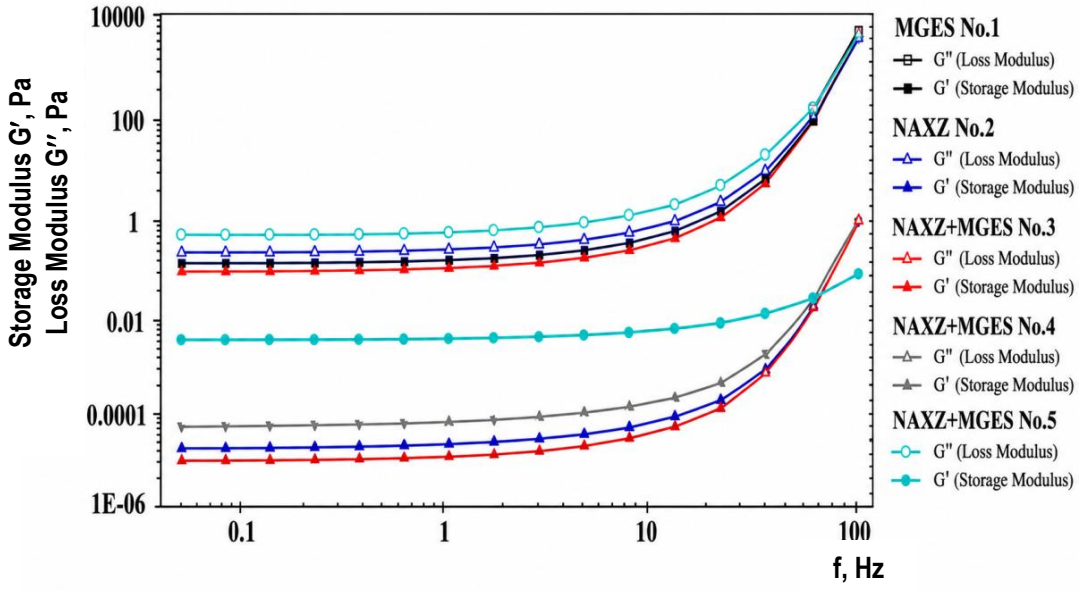

Figure 6. Dependence of the storage modulus (*G′*) and loss modulus (G″) on frequency (*f*)

This indicates that the systems of samples No. 4–5 behave as viscoelastic liquids with the presence of partially developed intermolecular structures. At frequencies around 6–10 rad s^{-1}, a sharp decrease in G' (from 0.002022 to 2.85×10^{-5} Pa) and a significant increase in tan δ (up to ≈20000) were observed. This behavior can be attributed to the breakdown and destabilization of the network structure in these systems. The relaxation time is relatively short, approximately 1–3 s. Because samples No. 4–5 exhibit viscoelastic solution behavior, their spraying performance and adhesion to mulberry leaves are expected to be higher than those of samples No. 1–3. At higher frequencies, all samples (No. 1–5) show characteristics typical of flowing liquid systems.

Thus, the rheological frequency analysis shows that in the initial samples No. 1–3, the dominance of G'' and the very high values of tan δ confirm the predominantly viscous character of the system and the absence of a stable macromolecular network. In contrast, for samples No. 4–5, the noticeable values of G' at low frequencies indicate the formation of a temporary dynamic network structure. With increasing frequency, this network gradually breaks down and the system transitions to a dissipative regime. Such behavior is characteristic of biopolymer systems stabilized by electrostatic interactions and hydrogen bonding.

In addition, the changes in dynamic viscosity (η, mPa·s) and shear stress (τ, Pa) of MHEC, CSNA, and their mixed solutions with increasing shear rate (γ, s^{-1}) were investigated, and the results are presented in Table 2.

Table 2

Dependence of shear stress (τ) and viscosity (η) on shear rate (γ) for samples No. 1–5

γ, s^{-1}	No. 1		No. 2		No. 3		No. 4		No. 5	
	τ	η	τ	η	τ	η	τ	η	τ	η
0.100	0.001	5.730	–	–	0.000	3.167	–	–	0.005	45.740
0.171	0.001	6.591	–	–	0.000	2.506	–	–	0.008	45.416
0.291	0.002	7.167	–	–	0.001	2.250	0.002	6.257	0.013	45.031
0.497	0.004	7.541	–	–	0.001	2.176	0.003	6.257	0.022	44.577
0.849	0.007	7.784	0.000	0.340	0.002	2.197	0.005	6.257	0.037	44.042
1.450	0.012	7.945	0.001	0.421	0.003	2.275	0.009	6.257	0.063	43.408
2.470	0.020	8.054	0.001	0.502	0.003	2.393	0.015	6.257	0.106	42.656
4.230	0.034	8.134	0.003	0.599	0.006	2.537	0.026	6.257	0.177	41.773
7.210	0.059	8.197	0.005	0.714	0.011	2.705	0.045	6.257	0.294	40.731
12.300	0.102	8.249	0.010	0.851	0.020	2.891	0.077	6.257	0.487	39.506
21.000	0.175	8.294	0.021	1.014	0.036	3.097	0.132	6.257	0.801	38.068
35.800	0.299	8.336	0.043	1.209	0.065	3.320	0.224	6.257	1.306	36.388
61.300	0.514	8.376	0.088	1.442	0.119	3.561	0.383	6.258	2.108	34.441
104.000	0.878	8.415	0.179	1.719	0.218	3.821	0.654	6.261	3.364	32.196
179.000	1.510	8.454	0.365	2.049	0.399	4.102	1.120	6.278	5.292	29.642
305.000	2.588	8.492	0.746	2.446	0.731	4.405	1.936	6.352	8.168	26.808
519.000	4.430	8.530	1.517	2.915	1.343	4.727	3.475	6.697	12.361	23.767
887.000	7.599	8.568	3.086	3.476	2.455	5.077	7.527	8.477	18.378	20.703
1510.000	13.034	8.606	6.275	4.143	–	–	16.568	10.941	27.243	17.993

Based on the data presented in Table 2, the experimental rheological properties of the studied solutions (samples No. 1–5) were investigated under steady shear conditions in order to quantitatively evaluate their flow behavior. For all samples, an increase in the shear rate (γ) from 0.1 to 1510 s^{-1} resulted in a corresponding increase in the shear stress (τ). The relationship between shear stress (τ) and shear rate (γ) was analyzed using the Power-law model. The parameters of this model provide important information about the internal structure and flow characteristics of the solution systems.

$$\tau = K\,\gamma^{n}, \tag{1}$$

where K is the consistency coefficient and n are the flow behavior index.

The calculated n and K parameters for the investigated solutions are presented in Table 3.

The value of the flow behavior index (n) allows evaluation of the non-Newtonian behavior of the system: when $n < 1$, the fluid exhibits pseudoplastic behavior; when $n = 1$, Newtonian behavior is observed; and when $n > 1$, the system demonstrates dilatant rheological behavior [18, 19]. The consistency coefficient (K)

characterizes the overall viscosity level of the solution, and an increase in its value indicates stronger intermolecular interactions within the system.

Table 3

Power-law rheological parameters (flow behavior index n, consistency index *K*) and correlation coefficients (R^2) for different CSNA/MHEC systems

No.	Sample composition	*n*	*K*, Pa·s^n	R^2	Rheological behavior
1	0.2 % MHEC	1.04	6.3	0.999	Dilatant
2	0.025 % CSNA	1.32	0.28	0.997–0.999	Strongly dilatant
3	0.0125 % CSNA : 0.1 % MHEC	1.11	2.4	0.998	Moderately dilatant
4	0.025 % CSNA : 0.2 % MHEC	1.00	6.2	0.999	Near-Newtonian behavior
5	0.05 % CSNA : 0.4 % MHEC	0.90	36	0.995-0.998	Pseudoplastic behavior

The obtained rheological parameters demonstrate variation in flow behavior ranging from dilatant to pseudoplastic depending on system composition. As can be seen from Table 3, for sample No. 1 (0.2 % MHEC), the values of $n = 1.04$ and $K = 6.3$ Pa·s^n were determined. Since the n value is slightly greater than 1, the solution exhibits weakly dilatant behavior. This indicates that the internal resistance of the solution increases with increasing shear rate. Such behavior can be explained by the orientation of the chains under shear, the formation of temporary associations between macromolecules, and an increase in the hydrodynamic volume.

For sample No. 2 (0.025 % CSNA), the values $n \approx 1.32$ and $K \approx 0.28$ Pa·s^n were observed. The considerably higher *n* value indicates strongly dilatant rheological behavior. In this case, an increase in shear rate enhances intermolecular interactions and promotes the formation of temporary structures between macromolecules. However, the relatively low *K* value indicates that the overall viscosity of the solution is comparatively low. This can be attributed to the low polymer concentration and the weak intermolecular interactions between macromolecules. For sample No. 3 (0.0125 % CSNA : 0.1 % MHEC), the values $n \approx 1.11$ and $K \approx 2.4$ Pa·s^n were determined for the complex system. This sample exhibits moderately dilatant behavior, which may result from weak interactions between CSNA and MHEC macromolecules, leading to the formation of temporary aggregates. Under shear conditions, these aggregates undergo rearrangement, which determines the rheological behavior of the solution. For sample No. 4 (0.025 % CSNA : 0.2 % MHEC), the values $n \approx 1.00$ and $K \approx 6.2$ Pa·s^n were observed.

The solution of this sample exhibits near-Newtonian rheological behavior. This indicates that the macromolecular structure of the system is relatively stable, and variations in shear rate do not significantly affect the viscosity. Such behavior can be explained by the uniform distribution of polymer chains, the presence of dynamic equilibrium between macromolecules, and the partial stability of the structure. For sample No. 5 (0.05 % CSNA : 0.4 % MHEC), the values $n \approx 0.90$ and $K \approx 36$ Pa·s^n were determined. Since $n < 1$, the system exhibits pseudoplastic rheological behavior, which is the most typical rheological regime for polymer solutions. With increasing shear rate, macromolecules become oriented, the chains are stretched, and the structure is partially disrupted, resulting in a decrease in viscosity. The relatively high *K* value indicates a higher polymer concentration in the solution, leading to stronger intermolecular associations and enhanced macromolecular interactions.

In addition, the Power-law model analysis showed that with increasing concentration in CSNA–MHEC systems, the flow behavior index (*n*) decreases. In low-concentration samples, $n > 1$, indicating dilatant behavior, whereas in higher-concentration systems $n < 1$ and higher *K* values confirm the formation of a dynamic spatial network. This suggests that the system possesses a structured viscoelastic dispersed nature.

To evaluate the quality of the approximation of rheological data, the power-law model was applied. It was found that the coefficients of determination (R^2) for all studied systems are in the range of 0.995–0.999, indicating an excellent agreement between the model and the experimental data. The relationship between viscosity (η) and shear rate (γ) is presented in Figure 7.

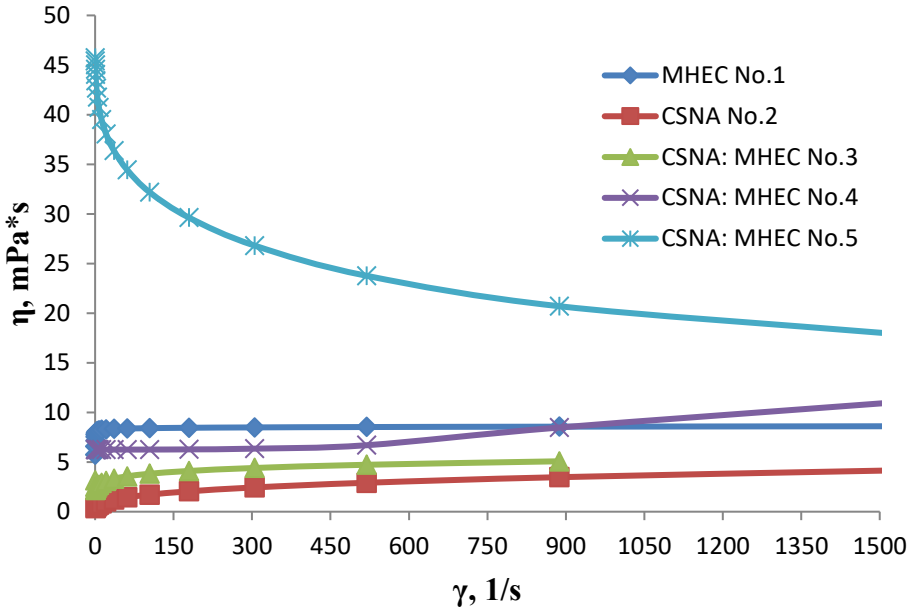

Figure 7. Dependence of viscosity (η) on shear rate (γ).

As can be seen from the graph, for sample No. 1 (0.2 % MHEC), when the shear rate increased from 0.1 to 1510 s^{-1}, the viscosity increased from 5.7 to 8.6 Pa·s. The increase in viscosity can be explained by the rearrangement of polymer chains in the direction of flow under shear and the increase in the number of entanglements, which leads to higher internal friction within the system.

A similar trend was observed for the 0.025 % CSNA solution (sample No. 2), where a gradual increase in viscosity under shear was detected (0.33 → 4.14 Pa·s). This behavior may be associated with hydrodynamic clustering of nanoparticles and the formation of temporary aggregates. Particle aggregation is governed not only by chemical attractive forces but also by hydrodynamic interactions arising from centrifugal forces under flow conditions. As a result, particles approach each other and form aggregates through weak intermolecular interactions.

For the low-concentration system (0.0125 % CSNA : 0.1 % MHEC, sample No. 3), a moderate increase in viscosity was observed (3.1 → 5.0 Pa·s). This behavior indicates the presence of certain interactions between the polymer chains and nanoparticles; however, a fully developed spatial network structure is not formed.

The medium-concentration system (0.025 % CSNA : 0.2 % MHEC, sample No. 4) exhibited near-Newtonian behavior, where the viscosity showed only a weak dependence on the shear rate (6.2 → 10.9 Pa·s). This can be explained by the rapid dynamic recovery of the solution structure. The highest concentration system (0.05 % CSNA : 0.4 % MHEC, sample No. 5) demonstrated pseudoplastic behavior. In this case, the viscosity decreased from 45 Pa·s to 18 Pa·s with increasing shear rate. This indicates the presence of a three-dimensional structure in the solution and its partial disruption under shear conditions.

The investigated solutions exhibited different rheological behaviors. In the case of MHEC and low-concentration CSNA samples, an increase in viscosity with increasing shear rate was observed. This behavior can be explained by hydrodynamic interactions between macromolecules and the strengthening of internal friction in the system due to molecular associations.

In contrast, in medium-concentration systems, the spatial network structure is not sufficiently developed; therefore, the resistance to flow changes only slightly, resulting in dilatant or near-Newtonian rheological behavior. Such rheological characteristics are favorable for the formation of stable dispersions in the spraying technologies used for agricultural preparations.

In high-concentration CSNA–MHEC solutions, pseudoplastic behavior was observed, indicating the formation of a temporary spatial network resulting from interactions between macromolecules and nanoparticles in the system. This structure is stabilized by hydrogen bonding, electrostatic interactions, and macromolecular associations. As a result, under increasing shear rate, the macromolecules become rearranged, leading to a decrease in viscosity and the manifestation of non-Newtonian rheological behavior.

Sample No. 4 (0.025 % CSNA : 0.2 % MHEC) exhibits near-Newtonian rheological behavior, where viscosity is almost independent of shear rate ($\eta \approx$ const). The macromolecular system remains stable, and temporary aggregates are continuously reformed. Due to the structural stability and uniform viscosity, nanoparticles are efficiently retained during the spraying process, and the solution can be easily applied.

In dilatant systems ($n > 1$), viscosity increases with shear rate due to the formation of transient associations, which complicates spraying. In contrast, pseudoplastic systems ($n < 1$) exhibit partial structural breakdown at high shear rates, requiring additional process control. Power-law model analysis ($n \approx 1$, $K \approx 6.2$ Pa·s^n) confirms that the solution possesses stable viscoelastic properties and ensures high efficiency during application.

4 Conclusions

The results of the study demonstrated that the rheological properties of CSNA–MHEC systems strongly depend on polymer concentration and composition. At low concentrations (0.0125–0.025 % CSNA), a gradual increase in viscosity under shear (0.33 → 5.0 Pa·s) was observed, indicating the formation of transient aggregates between macromolecules and nanoparticles. Systems with intermediate concentrations (0.025 % CSNA : 0.2 % MHEC) exhibited near-Newtonian behavior, confirming the presence of a dynamically reversible structure. In contrast, high-concentration systems (0.05 % CSNA : 0.4 % MHEC) showed pseudoplastic behavior and the formation of a three-dimensional network, accompanied by a partial decrease in viscosity and structural disruption under shear.

Power-law model analysis revealed that the flow behavior index (n) exceeds unity at low concentrations and decreases below unity at higher concentrations, while the increase in the consistency index (K) reflects stronger interactions between polymer chains and nanoparticles, as well as the formation of a dynamic spatial network. The high coefficients of determination ($R^2 = 0.995$–0.999) confirm the excellent agreement between the model and experimental data. Overall, the CSNA–MHEC systems exhibit stable viscoelastic and structured dispersed properties, which are of significant importance for the development of stable and structured polymer formulations in agriculture and pharmaceutical applications.

The results of DLS and AFM analyses confirmed the formation of nanoscale CSNA particles with sizes in the range of 200–700 nm. The DLS data revealed a dominant fraction of particles around 300–400 nm, corresponding to CSNA macromolecular structures, while larger particles (700–2672 nm) were attributed to MHEC. The good agreement between DLS and AFM results indicates the reliability of the obtained data. Overall, the polymeric preparative form represents a heterogeneous system consisting of CSNA nanoparticles and MHEC macromolecular structures.

*Author Information**

**The authors' names are presented in the following order: First Name, Middle Name and Last Name*

Oynavod Barotovna Avazova — Junior Researcher, Institute of Chemistry and Physics of Polymers of the Academy of Sciences of the Republic of Uzbekistan, 7B A. Kadyri St., 100128, Tashkent, Uzbekistan; e-mail: avazova1972@mail.ru, https://orcid.org/0000-0003-4552-6973

Kudrat Kadambayevich Pirniyazov (*corresponding author*) — Junior Researcher, Institute of Chemistry and Physics of Polymers of the Academy of Sciences of the Republic of Uzbekistan, 7B A. Kadyri St., 100128, Tashkent, Uzbekistan; e-mail: qudratpirniyazov8875@gmail.com, https://orcid.org/0009-0005-7014-7686

Sayyora Sharafovna Rashidova — Academician of the Academy of Sciences of the Republic of Uzbekistan, Doctor of Chemical Sciences, Professor, Head of the Laboratory "Synthesis of Advanced Polymers", Institute of Polymer Chemistry and Physics, Academy of Sciences of the Republic of Uzbekistan, 7B A. Kadyri St., 100128, Tashkent, Uzbekistan; e-mail: polymer@academy.uz, https://orcid.org/0000-0003-3104-6004

Author Contributions

The manuscript was written through contributions of all authors. All authors have given approval to the final version of the manuscript. CRediT: **Kudrat Kadambayevich Pirniyazov** conceptualization, data curation, investigation, methodology, validation, visualization, writing-review & editing; **Oynabod Boratovna Avazova** data curation, formal analysis, visualization; **Sayyora Sharafovna Rashidova** conceptualization,

data curation, formal analysis, funding acquisition, resources, supervision, validation, writing-original draft, writing-review & editing.

Acknowledgments

The work was carried out at the expense of the Institute's budget (Institute of Polymer Chemistry and Physics, Academy of Sciences of the Republic of Uzbekistan, Tashkent, Uzbekistan).

Conflicts of Interest

The authors declare no conflict of interest.

References

1 Milusheva, R. Yu., & Rashidova, S. Sh. (2019). *Bombyx Mori* Chitosan Nanoparticles: Synthesis and Properties. *Open Journal of Organic Polymer Materials, 09*(04), 63–73. https://doi.org/10.4236/ojopm.2019.94004

2 Pirniyazov, K.K., Milusheva, R.Yu., Rashidova, S.Sh. (2023). Production and biological activity of chitosan nanoascorbate. *INEOS OPEN, 6*(6), 156–162. https://doi.org/10.32931/io2326r

3 Pirniyazov, K.K., Rashidova, S.Sh. (2020). Synthesis of Ascorbate and Chitosan Nanoascorbate and Their Biologically Active Properties. *Journal of Science and Innovative Development, 3*(5), 47–62. https://doi.org/10.36522/2181-9637-2020-5-6

4 Pirniyazov, K.K., Tixonov, V.E., Rashidova, S.Sh. (2021). Synthesis and properties of oligochitosan ascorbate from *Bombyx mori*. *Bulletin of the Karaganda University. Chemistry Series*, 1(101), 91–98. https://doi.org/10.31489/2021Ch1/91-98

5 Wang, W., Meng, Q., Li, Q., Liu, J., Zhou, M., Jin, Z., & Zhao, K. (2020). Chitosan Derivatives and Their Application in Biomedicine. *International Journal of Molecular Sciences, 21*(2), 487. https://doi.org/10.3390/ijms21020487

6 Pirniyazov, K.K., Asrakulova, D.I., Rashidova, S.Sh. (2024). Synthesis and antimicrobial properties of chitosan nanoascorbate of *Bombyx mori*. *Moscow University Chemistry Bulletin, 79*(5), 345–350. https://doi.org/10.3103/S002713142470038X

7 Tian, X.L., Tian, D.F., Wang, Z.Y., Mo, F.K. (2009). Synthesis and evaluation of chitosan-vitamin C complex. *Indian J. Pharm Sci., 71*(4), 371–376. https://doi.org/10.4103/0250-474X.57284

8 Liping, L., Kexin, L., Huipu, D., Jia, L., Jie, Z. (2020). Study on Preparation of a Chitosan/Vitamin C Complex and Its Properties in Cosmetics. *Natural Product Communications*, 15, 1–9. https://doi.org/10.1177/1934578X20946876

9 Hafsa, J., Charfeddine, B., Smach, M.A., Limem, K., Majdoub, H., Sonia, R. (2014). Synthesis, characterization, antioxidant and antibacterial proprieties of chitosan ascorbate. *International Journal of Pharmaceutical and Chemical Sciences*, 4, 1072–1081. https://www.ijpcbs.com/articles/synthesis-characterization-antioxidant-and-antibacterial-proprieties-of-chitosan-ascorbate.pdf

10 Muzzarelli, R.A.A., Tanfani, F., Emanuelli, M. (1984). Chelating Derivatives of Chitosan Obtained by Reaction with Ascorbic Acid. *Carbohydrate Polymers, 4*(2), 137–151. https://doi.org/10.1016/0144-8617(84)90020-1

11 Zhuang, L., Zhi, X., Du, B., Yuan, S. (2020). Preparation of Elastic and Antibacterial Chitosan–Citric Membranes with High Oxygen Barrier Ability by in Situ Cross-Linking. *ACS Omega*, 5, 1086–1097. https://doi.org/10.1021/acsomega.9b03206

12 Yalinca, Z., Yilmaz, E., Taneri, B., Bullici, F., Tuzmen, S.J. (2013). Blood contact properties of ascorbyl chitosan. *Journal of Biomaterials Science, Polymer Edition*, 24, 1969–1987. https://doi.org/10.1080/09205063.2013.816929

13 Othman, N., Masarudin, M.J., Kuen, C.Y., Dasuan, N.A., Abdullah, L.C., Jamil, S.N.A. Md. (2018). Synthesis and Optimization of Chitosan Nanoparticles Loaded with l-Ascorbic Acid and Thymoquinone. *Nanomaterials*, 8, 920. https://doi.org/10.3390/nano8110920

14 Soliman, A., Gad, A. (2020). The Impact of Ascorbic Acid, Some Nanomaterials and Their Mixtures on Some Biological and Physiological Parameters of the Mulberry Silkworm *Bombyx mori L*. *Alexandria Science Exchange Journal*, 41, 393–398. https://doi.org/10.21608/asejaiqjsae.2020.119307

15 Ren, H., Liu, Y., Arshad, M., Dou, Z., Han, X. (2024). Effect of formulations and adjuvants on the properties of acetamiprid solution and droplet deposition characteristics sprayed by UAV. *Frontiers in Plant Science*, 15, 1441193. https://doi.org/10.3389/fpls.2024.1441193

16 Basílio, S., Furtado, Júnior, M.R., Alvarenga, C.B., da Vitória, E.L., Costalonga Vargas, B., Privitera, S., Caruso, L., Cerruto, E., Manetto, G., Caruso, L. (2024). Effect of adjuvants on physical–chemical properties, droplet size and drift reduction potential in agricultural spraying. *Agriculture*, 14(12), 2271. https://doi.org/10.3390/agriculture14122271

17 Hu, P., Zhang, R., Chen, L., Li, L., Tang, Q., Yan, W., Yang, J. (2024). Effect of polymer adjuvant type and concentration on atomization characteristics of agricultural spray nozzles. *Agriculture*, 14(3), 404. https://doi.org/10.3390/agriculture14030404

18 Mewis, J., Wagner, N.J. (2012). Colloidal suspension rheology. *Advances in Colloid and Interface Science*, 147–148, 214–227. https://doi.org/10.1016/j.cis.2008.09.005

19 Barnes, H.A. (1997). Thixotropy—a review. *Journal of Non-Newtonian Fluid Mechanics, 70*(1–2), 1–33. https://doi.org/10.1016/S0377-0257(97)00004-9

20 Butler Ellis, M.C., Tuck, C.R. (1999). How adjuvants influence spray formation with different hydraulic nozzles. *Crop Protection, 18*(2), 101–109. https://doi.org/10.1016/S0261-2194(98)00098-5

21 Zhao, H. and Liu, H. (2019). Breakup Morphology and Mechanisms of Liquid Atomization. Environmental Impact of Aviation and Sustainable Solutions, *IntechOpen*, 1-19. https://doi.org/10.5772/intechopen.84998

22 Mun, R.P., Young, B.W., Boger, D.V. (1999). Atomisation of dilute polymer solutions in agricultural sprays. *Journal of Non-Newtonian Fluid Mechanics, 83*(1–2), 163–178. https://doi.org/10.1016/S0377-0257(98)00130-7

23 Rinaudo, M. (2006). Chitin and chitosan: Properties and applications. *Progress in Polymer Science, 31*(7), 603–632. https://doi.org/10.1016/j.progpolymsci.2006.06.001

24 Pirniyazov, K.K., Nurgaliyev, I.N., Rashidova, S.Sh. (2023). Reaction of the Formation of Chitosan Nanoascorbate *Bombyx Mori* and Computer Simulation of Its Structure. *Intelligent Biotechnologies of Natural and Synthetic Biologically Active Substances AIP Conference Proceedings*, 2931, 060002-1–060002-9. https://doi.org/10.1063/5.0182628

25 Kumar, M.N.V.R. (2000). A review of chitin and chitosan applications. *Reactive and Functional Polymers, 46*(1), 1–27. https://doi.org/10.1016/S1381-5148(00)00038-9

26 Fan, W., Yan, W., Xu, Z., Ni, H. (2012). Formation mechanism of monodisperse, low molecular weight chitosan nanoparticles by ionic gelation technique. *Colloids and Surfaces B: Biointerfaces*, 90, 21–27. https://doi.org/10.1016/j.colsurfb.2011.09.042

27 Younes, I., Rinaudo, M. (2015). Chitin and chitosan preparation from marine sources: Structure, properties and applications. *Marine Drugs*, 13(3), 1133–1174. https://doi.org/10.3390/md13031133

28 Desai, M.P., Labhasetwar, V., Amidon, G.L., Levy, R.J. (1996). Gastrointestinal uptake of biodegradable microparticles: effect of particle size. *Pharmaceutical Research*, 13(12), 1838–1845. https://doi.org/10.1023/a:1016085108889